ChemPubSoc Europe

DOI: 10.1002/cphc.201402016

Phosphate Monoester Hydrolysis by Trinuclear Alkaline Phosphatase; DFT Study of Transition States and Reaction Mechanism

Shi-Lu Chen*[a] and Rong-Zhen Liao*[b]

Alkaline phosphatase (AP) is a trinuclear metalloenzyme that catalyzes the hydrolysis of a broad range of phosphate monoesters to form inorganic phosphate and alcohol (or phenol). In this paper, by using density functional theory with a model based on a crystal structure, the AP-catalyzed hydrolysis of phosphate monoesters is investigated by calculating two substrates, that is, methyl and *p*-nitrophenyl phosphates, which represent alkyl and aryl phosphates, respectively. The calculations confirm that the AP reaction employs a "ping-pong" mechanism involving two chemical displacement steps, that is, the displacement of the substrate leaving group by a Ser102 alkoxide and the hydrolysis of the phosphoseryl intermediate by a Zn2-bound hydroxide. Both displacement steps proceed via a concerted associative pathway no matter which substrate is used. Other mechanistic aspects are also studied. Comparison of our calculations with linear free energy relationships experiments shows good agreement.

1. Introduction

Alkaline phosphatase (AP) is a hydrolase responsible for removing phosphate groups from various types of molecules including nucleotides, proteins, and alkaloids.[1–3] It is a trinuclear metalloenzyme (one magnesium and two zinc atoms) that catalyzes the hydrolysis of a broad range of phosphate monoesters to produce inorganic phosphate (Pi) and alcohol (or phenol) under both acidic and alkaline conditions (Scheme 1).[1–3] It is an almost perfect, that is, nearly diffusion-limited, enzyme,[4–5] with a k_{cat}/K_m (turnover number/Michaelis constant) value of $(3.3\pm0.5)\times10^7\,\text{M}^{-1}\text{s}^{-1}$ for *p*-nitrophenyl phosphate substrate at room temperature.[6] AP also displays the catalytic promiscuity with a lower level of phosphodiesterase activity.[7,8] It has been an interesting system for the characterization of transition states in enzymatic hydrolysis of phosphate esters, for the investigation of catalytic properties of binuclear zinc hydrolases,[1,9–16] and also for the study of enzyme promiscuity and evolution.[17–19]

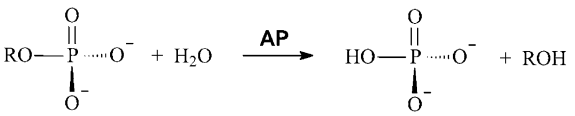

Scheme 1. Hydrolysis of phosphate monoesters catalyzed by alkaline phosphatase (AP).

AP from *Escherichia coli* has been extensively characterized using a variety of mechanistic, kinetic, genetic, structural, and spectroscopic approaches. Various crystal structures of AP have been obtained, including the free enzyme (PDB code: 1ED8),[20] AP with diverse inhibitors bound,[20,21] and the covalent phosphoenzyme intermediate.[22] AP is a homodimeric metalloenzyme containing two zinc ions and one magnesium ion in each active site (Figure 1). The two zinc ions are separated by ~4 Å and bound to the protein through the side chains of His331, His412, Asp327, Asp369, and His370. The carboxylate group of Asp51 acts as a bridge to connect Zn1 with Mg. The Mg ion is bound with octahedral geometry and, besides Asp51, it is ligated by Glu322, Thr155, and three water molecules. The Pi sits in the pocket between two zinc ions and is interacting with Arg166 through two hydrogen bonds.[7] The mutation of this arginine residue to an alanine does not inactivate the enzyme[7,23] but shows that Arg166 is possibly accountable for the preference of AP for phosphate monoesters.[7] The investigation of the reaction of the A166S mutant indicates that this Arg166 residue does not substantially change the leaving group dependence and hardly affects the character of the transition state.[24] Ser102, which is reported to have a pK_a of ≤ 5.5 in the free enzyme,[6] appears to function as the crucial nucleophile to attack the phosphorus center during the reaction.[12,13,20] In the crystal structure of the wild-type AP (PDB entry 1ED9),[20] one of the water molecules (**W3** in Figure 1) coordinated to Mg^{2+} is in close proximity to Zn1 (4.7 Å) and the

[a] *Prof. S.-L. Chen*
Key Laboratory of Cluster Science of Ministry of Education
Beijing Key Laboratory of Photoelectronic/Electrophotonic Conversion Materials, School of Chemistry
Beijing Institute of Technology, Beijing 100081 (China)
Fax: (+86) 01-6891-1354
E-mail: shlchen@bit.edu.cn

[b] *Dr. R.-Z. Liao*
Department of Organic Chemistry
Arrhenius Laboratory, Stockholm University
10691 Stockholm (Sweden)
E-mail: rongzhen@organ.su.se

Supporting Information for this article is available on the WWW under http://dx.doi.org/10.1002/cphc.201402016.

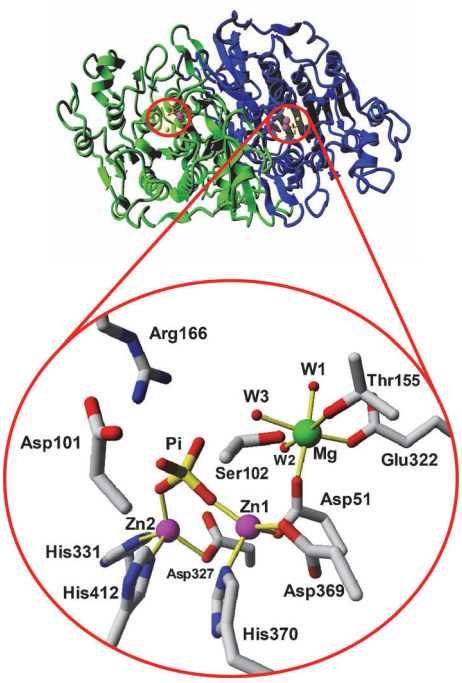

Figure 1. Overall view of the AP structure and close-up view of the active site with an Pi bound. Coordinates from PDB entry 1ED8[20] were used to generate the pictures. The water molecules coordinated to Mg are referred to as W1, W2, and W3.

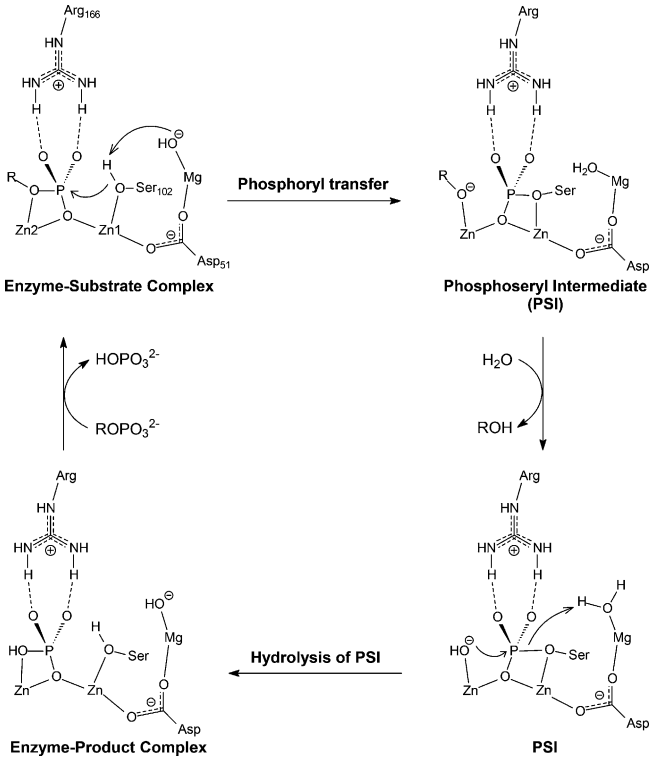

Scheme 2. Proposed reaction mechanism of AP.

oxygen of Ser102 (3.1 Å). This water molecule is suggested to deprotonate to a hydroxide ion ($O_{Mg}H^-$) by the solution[20,25–27] and is proposed to work as a general base/acid for regulating the protonation state of Ser102.[11,15,20] The Mg^{2+} ion is examined to prefer octahedral coordination, which is suggested to be able to structurally stabilize the active site in a catalytically most active conformation.[28]

By using X-ray crystallographic techniques, the structures of various steps in the catalytic cycle of AP have been captured, including 1) the free enzyme in the absence of Pi,[20] 2) the covalent phosphoenzyme intermediate,[22] 3) the enzyme with a transition state analog bound,[21] and 4) the non-covalent enzyme–Pi complex.[20] Based on these X-ray crystal structures, a three-metal reaction mechanism has been proposed, suggesting that two in-line displacements occur at the phosphorus center (see Scheme 2).[20] The first in-line attack comes from the Ser102 alkoxide[1,20,21], which is activated by the hydroxide that is stabilized by the Mg ion ($O_{Mg}H^-$).[20,25] This leads to a negatively charged leaving group (alkoxide or phenolate) stabilized by the Zn2 ion. This displacement step results in a covalent phosphoseryl intermediate (**PSI**) and is thus called phosphoryl transfer. Then, a solvent water molecule comes in and protonates the leaving group, leading to free alcohol (or phenol) product and a Zn2-bound hydroxide ($O_{Zn2}H^-$). Next, the resulting $O_{Zn2}H^-$ performs the second in-line attack to yield the enzyme–Pi product complex,[20] simultaneously regenerating the Ser102 and $O_{Mg}H^-$.[1,20] This "ping-pong" mechanism proceeds with retention of the configuration at the phosphorus center, which has been confirmed by isotope-labeling experiments.[3]

Characterization of the transition states that are involved in the reaction is a useful way to understand enzymatic catalysis. A number of studies using linear free energy relationships (LFERs) have been performed with respect to AP reactions, but they provide quite different information about the nature of the transition states.[6,29–32] For example, the AP-catalyzed hydrolysis of aryl O-phosphorothiolates has been observed to have a steep leaving-group dependence (the Brønsted value $\beta = -0.77$),[29] indicating that the transition state is largely dissociative.[9,29] In contrast, the studies using aryl phosphates showed that the turnover number (k_{cat}) was almost independent of the pK_a of the leaving group and nearly constant.[6,30–32] For alkyl phosphates, earlier studies found little dependence upon the nature of the leaving group.[30,32] In contrast, a study, which employed a more sensitive ^{32}P-based assay argued that the dependence of k_{cat}/K_m on the pK_a of the leaving group follows a steep Brønsted correlation with $\beta = -0.85$.[6] Interestingly, a theoretical study of the phosphate ester hydrolysis in aqueous solution showed similar barriers for associative and dissociative pathways.[33] It was thus suggested that an enzyme active site could select either of these mechanisms depending on the particular electrostatic environment.[33]

Several theoretical studies have been performed to characterize transition states and interpret the mechanism of AP.[17–19,28,34] One of them employed a quantum mechanics/molecular mechanics (QM/MM) method with a semiempirical AM1/d-PhoT method in the QM part and proposed an either associative or dissociative reaction mechanism for the hydrolysis of *p*-nitrophenyl phosphate depending on the size of the QM subsystem.[34] It suggested that the inclusion of metal atoms and

their coordination spheres in the QM model would change the mechanism from concerted associative to stepwise dissociative pathways. This study shows a note of caution when using QM/MM methods, that is, different mechanism can be obtained if an inadequate QM/MM partition is done. In another QM/QM-ONIOM (our own *n*-layered integrated molecular orbital and molecular mechanics) investigation, in which metal atoms, a methyl phosphate, five water molecules, one hydroxide, the carboxylates of glutamates and aspartates, and the CH_2OH groups of serines were included in the high layer and calculated by using density functional theory (DFT) with the B3LYP functional,[35–37] the nucleophilic attack of the serine alkoxide on the phosphorus atom was proposed to be the rate-limiting step for the hydrolysis of methyl phosphate.[28] Recently, two QM/MM computations using AM1/d-PhoT[18] and approximate DFT (SCC-DFTBPR)[17] methods in the QM parts were carried out for phosphate diester substrates and implied the catalytic promiscuity of the AP superfamily. QM/MM simulations by Moliner, Tuñón and co-workers found a dissociative mechanism for diester hydrolysis and the Zn–Zn distance is about 5.7 Å in the transition state,[18] whereas Hou and Cui found an associative mechanism and the corresponding Zn–Zn distance is about 4.0 Å.[17] The most recent QM/MM analysis by Hou and Cui suggested that in both R166S AP and nucleotide pyrophosphatase/phosphodiesterase (NPP) the hydrolysis of the phosphate monoester (*p*-nitrophenyl phosphate) involves looser transition states compared to the hydrolysis of the phosphate diester.[19] Therefore, they proposed that AP enzymes are able to recognize and stabilize different types of transition states in a single active site.[19] The modeling challenges of promiscuity in the alkaline phosphatase superfamily have been very recently discussed by Kamerlin and co-workers.[38]

To gain deeper insight into the hydrolysis of phosphate monoesters catalyzed by AP, using the DFT with the hybrid B3LYP function,[35–37] in the present work we have calculated the AP-catalyzed reactions of two substrates, that is, methyl and *p*-nitrophenyl phosphates, which represent alkyl and aryl phosphate substrates, respectively. The potential energy surfaces (PES) for the two substrates are presented and the characterization of the transition states and intermediates involved are provided. The same computational approach has been used previously to study the reaction mechanisms of a number of multinuclear zinc enzymes, such as phosphotriesterase (PTE),[39–41] aminopeptidase from *Aeromonas Proteolytica*,[42] glyoxalase II,[43] methionine aminopeptidase,[44] human prolidase,[45] protein phosphatase 5,[46] arylsulfatase,[47] human arginase I,[48] cAMP-dependent protein kinase,[49] nuclease P1 (a trinuclear zinc enzyme),[50] and so forth. Our calculations demonstrate that the AP-catalyzed hydrolysis of methyl and *p*-nitrophenyl phosphates both proceed through a concerted associative pathway. Furthermore, it is revealed that both chemical displacement steps (phosphoryl transfer and hydrolysis of **PSI**) should contribute to the rate limitation in the AP-catalyzed hydrolysis of alkyl phosphates, whereas, in the hydrolysis of aryl phosphates, the first chemical step has a much lower barrier than that of the second step and the release of phenolate products from the AP active site may be rate-determining.

Computational Details

A model of the AP active site (see the structures $\mathbf{R_{me}}$ and $\mathbf{R_{pnp}}$ in Figures 2 and 3) was constructed on the basis of a crystal structure of the wild-type AP with phosphate bound (PDB code 1ED8).[20] In this case, it is expected that the use of a crystal structure with a phosphate inhibitor bound may provide an initial geometry as close as the enzyme-substrate complex. The model contains the two zinc ions, the magnesium ion, His331, His412, Asp327, Asp369, His370, Asp51, Glu322, Thr155, Arg166, Ser102, two water molecules ligated to Mg, and a Mg-stabilized OH^- ($O_{Mg}H^-$). The negatively charged Asp101, a second-shell residue that makes strong

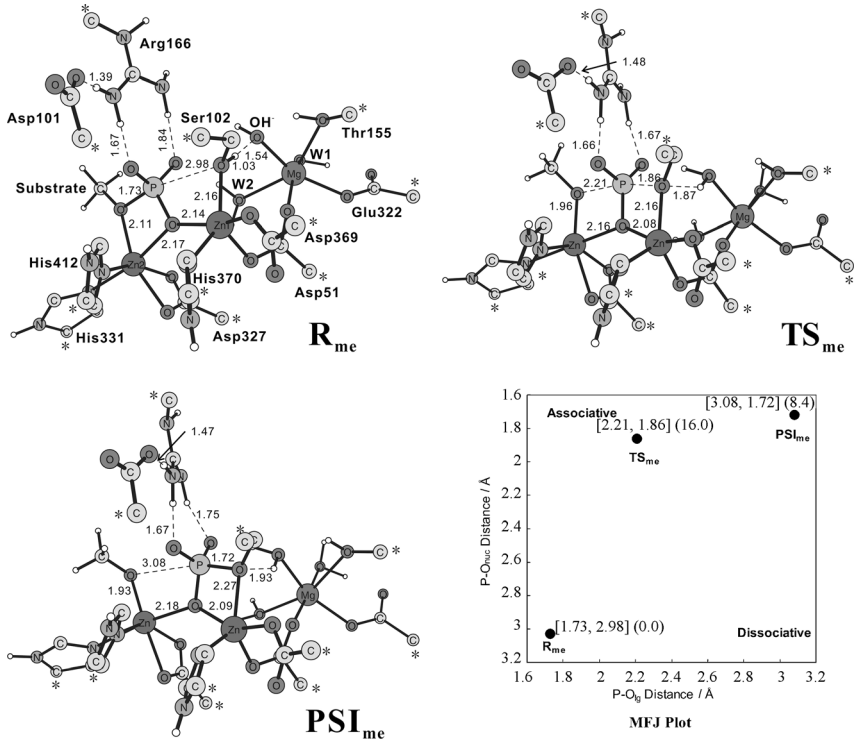

Figure 2. Optimized structures of stationary points along the phosphoryl transfer pathway in the methyl phosphate hydrolysis and the corresponding More–O'Ferral–Jencks (MFJ) plot. For clarity, a few hydrogen atoms are omitted. Asterisks indicate the atoms that are fixed to their X-ray positions. All distances are indicated in angstrom [Å]. In the MFJ plot, the key distances of the phosphor to the leaving group oxygen ($P–O_{lg}$) and the nucleophile oxygen ($P–O_{nuc}$) are given in square brackets, and relative energies [kcal mol^{-1}] are provided in parentheses.

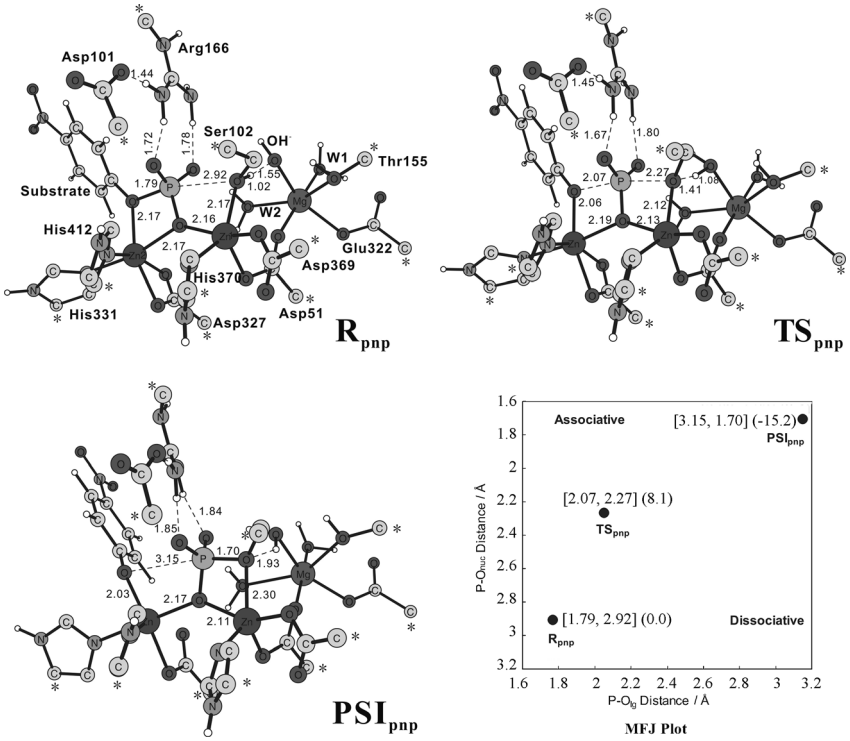

Figure 3. Optimized structures of stationary points along the phosphoryl transfer pathway in the *p*-nitrophenyl phosphate hydrolysis and the corresponding More–O'Ferrall–Jencks (MFJ) plot. For clarity, a few hydrogen atoms are omitted.

hydrogen bonds to the positively charged Arg166, is also included in the model. To reduce the size of the model, amino acids were truncated so that, in principle, only side chains were kept in the model. The histidines were thus presented by imidazoles, aspartates by acetates, glutamate by acetate, threonine by methanol, serine by ethanol, and arginine by *N*-methyl-guanidine. The atoms for which the truncation was done were kept frozen to their X-ray crystal positions during optimizations to preserve the spatial arrangement of the residues. These centers are indicated by asterisks in Figures 2 and 3. In a previous study on the related phosphotriesterase enzyme, it has been shown that this procedure works well because the effects on the energy profile are not very large.[41] A scrutiny into the hydrolysis of only one substrate is, however, not sufficient to give a panorama of the AP reaction, as the enzymatic hydrolysis of phosphate esters has been shown to be rather complicated; even a small alteration of the acidity of the leaving group may change the transition-state nature.[51,52] Therefore, in this paper, we examined the hydrolysis of two substrates, methyl and *p*-nitrophenyl phosphates, which represent alkyl and aryl phosphates, respectively. The total charge of the model is −1 and the total numbers of atoms are 110 and 119 for the methyl and the *p*-nitrophenyl phosphate-bound systems, respectively. This model is now considered to be relatively small, and the flexibility is thus limited. However, as discussed below, the solvation effects on the energetics are small. This indicates that most polarization has been captured by the present model and a non-neutral model (overall charge = −1) does not lead to problematic results.

All calculations were performed by using the DFT functional B3LYP[35–37] as implemented in the Gaussian 03 program package.[53] Geometry optimizations were carried out with the 6-31G(d,p) basis set for the C, H, O, N, P, and Mg elements and with the effective core potential LANL2DZ basis set for Zn. Based on these optimized geometries, more accurate energies were obtained by performing single-point calculations with the larger basis set 6-311 + G(2d,2p) for all elements.

To estimate the effects of the protein environment that is not explicitly included in the quantum chemical model, single-point calculations on the optimized structures were carried out with the conductor-like polarizable continuum model (CPCM)[54–57] method at the same level of theory as the geometry optimizations. The dielectric constant was chosen to be $\varepsilon = 4$, which is a standard value used in this kind of applications.[58] As seen from the potential energy surfaces shown in Figure 4 the solvation effects are small. In fact, it has recently been shown for several enzyme classes that the solvation effects diminish rapidly as a function of the model size.[59–62]

Frequency calculations were performed at the same theory level as the geometry optimizations to obtain the zero-point energies (ZPE) and to confirm the nature of the stationary points. As discussed above, some atoms were kept fixed to their X-ray crystal positions. This procedure gives rise to a few small imaginary frequencies. The number of imaginary frequencies is usually 5–8 with an amount of $< 30\ cm^{-1}$. These frequencies do not contribute significantly to the ZPE. An investigation of varying constraints with acetylene hydratase[63] as an example indicates that the coordinate error has very small effect on the calculated energies when the resolution of the starting crystal structure is better than 2.0 Å (1.75 Å

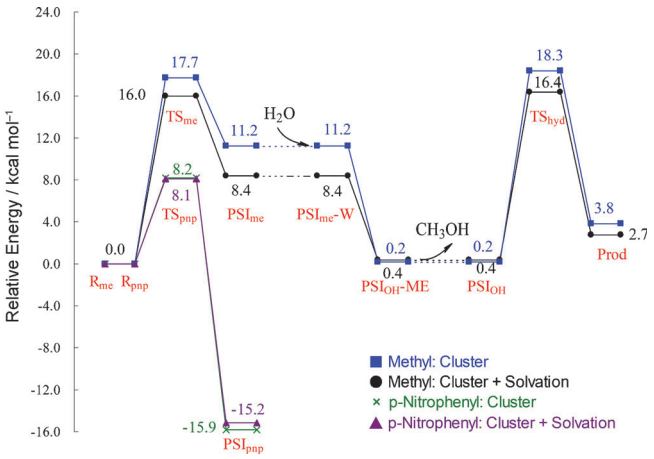

Figure 4. Calculated energy profiles for the AP-catalyzed reactions. Methyl: the hydrolysis of methyl phosphate. *p*-Nitrophenyl: the hydrolysis of *p*-nitrophenyl. Cluster: B3LYP/6-311 + G(2d,2p) energies with zero-point energies included. Solvation: CPCM solvation effects added.

in the present case). Another study of phosphotriesterase[41] also shows that the energy differences between with and without atom fixation are not of such a magnitude that they alter any conclusion about the mechanism. These imaginary frequencies should thus not affect the accuracy of the energies. However, they make the calculations of the harmonic entropy effects inaccurate. Therefore, entropy was not considered in the current study.

2. Results and Discussion

2.1. Optimized Reactant States

The optimized structures of the AP active site with methyl ($\mathbf{R_{me}}$) and *p*-nitrophenyl ($\mathbf{R_{pnp}}$) phosphates bound are displayed in Figures 2 and 3, respectively. The overall geometric parameters obtained from the geometry optimizations agree quite well with the X-ray structure. For example, the Zn1–Zn2 distances are calculated to be 4.03 and 4.00 Å for $\mathbf{R_{me}}$ and $\mathbf{R_{pnp}}$, respectively, to be compared to the crystallographic distance of 3.98 Å[20] and another crystallographic distance of 4.12 Å obtained recently (PDB code: 3TG0).[64] In these two enzyme–substrate complexes, the substrates are fastened by the Arg166 through two hydrogen bonds and the leaving groups are located at the position opposite to the Ser102. In addition, one of the phosphoryl oxygens, denoted by O_μ, is bridging the two zinc ions.

2.2. Methyl Phosphate Substrate

The phosphoryl transfer step, achieved by the attack of Ser102 alkoxide on the phosphorus center (Scheme 2), has been demonstrated by X-ray crystallography,[21,22] kinetic experiments,[65] and NMR spectroscopy.[66] The nucleophile, Ser102 alkoxide, is proposed to be activated by the hydroxide ($O_{Mg}H^-$) bound to Mg.[11,15,20] However, the origin of this crucial general base ($O_{Mg}H^-$) is still an open question. The most likely possibility is that the $O_{Mg}H^-$ derives from the deprotonation of a water molecule ligated to Mg by the hydroxide in solution. A similar example has been demonstrated in the phosphodiester hydrolysis catalyzed by DNA Polymerase I.[27]

In the AP-methyl phosphate complex, the oxygen of Ser102 (O_{nuc}) coordinates to the Zn1 ion and is separated from the phosphorus center by 2.98 Å (see $\mathbf{R_{me}}$ in Figure 2). From $\mathbf{R_{me}}$, a transition state (denoted by $\mathbf{TS_{me}}$) for the nucleophilic attack on the phosphor by the O_{nuc} has been located. The optimized structure of $\mathbf{TS_{me}}$ and the resulting phosphoseryl intermediate ($\mathbf{PSI_{me}}$) are shown in Figure 2. By frequency analysis, the nature of $\mathbf{TS_{me}}$ has been confirmed to be a first-order saddle point with an imaginary frequency of 116*i* cm^{-1}, which is related to a vibrational mode that the leaving group (methoxide, CH_3O^-) departs simultaneously with the attack of the O_{nuc} atom on the phosphor, indicating a concerted process. At $\mathbf{TS_{me}}$, the distances of the phosphor to the O_{nuc} (P-O_{nuc}) and the leaving group oxygen (P-O_{lg}) are 1.86 and 2.21 Å, respectively. Furthermore, it is observed that at $\mathbf{TS_{me}}$ the proton of Ser102 is also concertedly transferred to the $O_{Mg}H^-$ leading to an Mg-bound water molecule (H_2O_{Mg}). We could not locate an intermediate, where the proton of Ser102 has been delivered to the $O_{Mg}H^-$ but nucleophilic attack has not taken place yet. The phosphoryl transfer results in a tetra-coordinated phosphoenzyme intermediate ($\mathbf{PSI_{me}}$), in which a covalent bond between the phosphor and the Ser102 oxygen is formed (P–O_{nuc} = 1.72 Å) whereas the P–O_{lg} bond has been broken (3.08 Å). This $\mathbf{PSI_{me}}$ intermediate has been confirmed experimentally by X-ray crystallography.[22] The overlaid structure of $\mathbf{R_{me}}$, $\mathbf{TS_{me}}$, and $\mathbf{PSI_{me}}$ (see Figure S1 in the Supporting Information) shows a high degree of structural consistency and that the main structural changes happen in the reacting region (i.e. the part of substrate + Ser102 + $O_{Mg}H^-$). This confirms $\mathbf{TS_{me}}$ to be the transition state connecting the $\mathbf{R_{me}}$ and $\mathbf{PSI_{me}}$. The energetic barrier of phosphoryl transfer is calculated to be 17.7 kcal mol^{-1} in the cluster model (Figure 4). Upon the addition of solvation effects simulated in the form of CPCM (see details in the Computational Details), the barrier is slightly lowered to 16.0 kcal mol^{-1}. The $\mathbf{PSI_{me}}$ intermediate is calculated to lie 11.2 kcal mol^{-1} higher than the reactant complex of $\mathbf{R_{me}}$ (+8.4 kcal mol^{-1} with the solvation included).

To characterize the nature of phosphoryl transfer in the methyl phosphate hydrolysis, the PES is represented by a More–O'Ferrall–Jencks (MFJ) plot,[67,68] which defines the PES in terms of two reaction coordinates, that is, the P–O_{lg} and the P–O_{nuc} distances (see Figure 2). In the MFJ plot of Figure 2, the reactant ($\mathbf{R_{me}}$) is located at the bottom left corner and the intermediate ($\mathbf{PSI_{me}}$) is at top right. A stepwise associative pathway passes through the top left corner, at which a penta-coordinated phosphate intermediate is situated. In addition, a three-coordinated metaphosphate intermediate is sitting at the bottom right corner, through which a stepwise dissociative pathway proceeds. We place the obtained stationary points into the MFJ plot in terms of their P–O_{lg} and P–O_{nuc} distances, and the nature of the transition state ($\mathbf{TS_{me}}$) turns out to be associative. Therefore, it can be concluded that, in the AP-catalyzed hydrolysis of methyl phosphate, phosphoryl transfer proceeds along a concerted associative pathway. It should be mentioned here that many attempts have been made to find the dissociative pathways (concerted or stepwise) and the stepwise associative path, but without success.

It is of significance to check some geometrical changes that take place during phosphoryl transfer, as these can reflect important chemistry. At $\mathbf{TS_{me}}$, most of distances between the Zn ions and the oxygen atoms of phosphate moiety, including Zn1–O_μ, Zn2–O_{lg}, and Zn2–O_μ, are shortened compared to the $\mathbf{R_{me}}$ reactant (see Figure 2). This may indicate that the two Zn ions play a role in stabilizing the transition state, which is consistent with the conclusion drawn from the investigations of LFERs[69] and crystallography,[21] that is, the electrostatic interactions of the phosphate with Zn ions are critical factors for the stabilization of the transition-state structure. Another important parameter is the distance of Zn2 to the oxygen of the leaving group (Zn2–O_{lg}). From 2.11 Å in the enzyme–substrate complex ($\mathbf{R_{me}}$), the distance is decreased to 1.96 Å in $\mathbf{TS_{me}}$ and finally reaches 1.93 Å at the $\mathbf{PSI_{me}}$ structure. This implies that another role of Zn2 may be to stabilize the developing charge of the leaving group. It can also be observed that the changes of the two hydrogen-bond distances between Arg166 and the

phosphate moiety are small during phosphoryl transfer (Figure 2), suggesting that Arg166 only makes a slight contribution to the catalysis. This may explain why the mutation of this arginine residue does not inactivate the enzyme.[7,23]

2.3. *p*-Nitrophenyl Phosphate Substrate

In addition, the phosphoryl transfer of the *p*-nitrophenyl phosphate hydrolysis was investigated. From the enzyme–substrate complex (**R_{pnp}**, Figure 3), a transition state (**TS_{pnp}**) for the displacement of the leaving group (*p*-nitrophenolate) by the nucleophile (Ser102 alkoxide) was optimized. The obtained geometries of the transition state and the resulting phosphoseryl intermediate (**PSI_{pnp}**) are shown in Figure 3. The **TS_{pnp}** was proved by frequency analysis to be a first-order saddle point with an imaginary frequency of 233*i* cm^{-1}. The imaginary vibrational form indicates a concerted process, that is, concomitantly with the P–O_{nuc} bond formation, the P–O_{lg} bond is broken and the proton of Ser102 is transferred to the $O_{Mg}H^-$. At **TS_{pnp}**, the crucial P–O_{nuc} and P–O_{lg} distances are 2.27 and 2.07 Å, respectively. As in the case of methyl phosphate discussed before, in the **TS_{pnp}** structure most distances between the Zinc ions and the oxygen atoms of the phosphate moiety (including Zn1–O_{nuc}, Zn1–O_{μ}, and Zn2–O_{lg}) are shortened compared to the **R_{pnp}** structure (see Figure 3). This implies again that, in the transition states, the zinc ions may stabilize the structures better than in the enzyme–substrate complexes. This step leads to a phosphoenzyme intermediate (**PSI_{pnp}**, Figure 3) with a tetra-coordinated configuration at the phosphorus center. The analysis of structural consistency by overlaying **R_{pnp}**, **TS_{pnp}**, and **PSI_{pnp}** (Figure S2) indicates that these three stationary points are connected in the same reaction coordinate. The barrier of this process is calculated to be 8.1 kcal mol^{-1} including the solvation, which is significantly lower than that in the hydrolysis of methyl phosphate (Figure 4). In addition, it is calculated to be 23.3 kcal mol^{-1} downhill from the **TS_{pnp}** transition state to the **PSI_{pnp}** intermediate, making this step strongly exothermic by 15.2 kcal mol^{-1}. This can be rationalized by considering the pK_a values of the leaving groups. The *p*-nitrophenolate resulted in this step is a better leaving group compared to the methoxide owing to its low pK_a of 7.1.[71] This is able to largely lower the energy of the phosphoseryl intermediate and thus to decrease the reaction barrier. Consistent with the energetics, the **TS_{pnp}** is a much earlier transition state than the **TS_{me}** (see geometries in Figures 2 and 3). For example, the P–O_{nuc} distance of **TS_{pnp}** (2.27 Å) is much longer than that of **TS_{me}** (1.86 Å) whereas the P–O_{lg} distance (2.07 Å) is much shorter (2.21 Å at **TS_{me}**). However, it should be noted that the exothermicity difference between the two substrates (23.6 kcal mol^{-1}, Figure 4) is larger than the pK_a difference of the leaving group. This may be due to the limitation of the cluster model and the complicated surrounding of the AP active site. In particular, the nucleophilic Ser102 is inside the protein, whereas the leaving-group side of the AP active site is exposed to the solution.

It is worth noting the change of the distance between Zn2 and the leaving group oxygen (Zn2–O_{lg}) during the phosphoryl transfer of *p*-nitrophenyl phosphate hydrolysis. In going from the enzyme-substrate complex (**R_{pnp}**) to the phosphoseryl intermediate (**PSI_{pnp}**) via the transition state (**TS_{pnp}**), the Zn2–O_{lg} distance is shortened from 2.17 to 2.03 Å (via 2.06 Å at **TS_{pnp}**, Figure 3). This again provides evidence that the Zn2 ion may play a role in stabilizing the developing charge of the leaving group and consequently facilitating phosphoryl transfer.

Also here, we place the obtained stationary points in the corresponding MFJ plot according to their P–O_{lg} and P–O_{nuc} distances (Figure 3). From the MFJ plot, it can be observed that the phosphoryl transfer in the case of *p*-nitrophenyl phosphate also follows a concerted associative pathway, similar to methyl phosphate. And again, we could not find a dissociative or stepwise associative pathway. Particular attention has been paid to the sum of the P–O_{lg} and P–O_{nuc} distances at the transition state (i.e. P–O_{lg} + P–O_{nuc}). It can be seen that the value of "P–O_{lg} + P–O_{nuc}" in the hydrolysis of *p*-nitrophenyl phosphate (4.34 Å, Figure 3) is larger than that in the case of methyl phosphate (4.07 Å, Figure 2). This indicates that the nature of the phosphoryl transfer goes rather into the dissociative direction with the pK_a of the leaving group decreasing, although the nature has been shown above to be associative for both methyl and *p*-nitrophenyl phosphate systems. This conclusion is consistent with a previous investigation,[51] during which systematic calculations on the PESs of the reactions of a number of phosphate monoesters with different leaving groups has been performed.

2.4. Hydrolysis of Phosphoseryl Intermediate (PSI)

Once phosphoryl transfer is accomplished, the resulting methoxide (or *p*-nitrophenolate) may be protonated to release alcohol (or *p*-nitrophenol) product following two possible pathways. One is to react with a water molecule activated by a Zn2 ion and to generate a Zn2-stabilized hydroxide ($O_{Zn2}H^-$);[21] another way is that the methoxide is directly expelled into the solution and gets protonated there. For *p*-nitrophenolate, the protonation is probably not necessary at all. The $O_{Zn2}H^-$, which acts as the nucleophile in the second chemical step of the phosphoseryl intermediate hydrolysis, may come from the solution directly. The exposure of the leaving-group side of the active site to the solution, as indicated by AP crystals, structurally ensures the feasibility of the two pathways mentioned above. After the alcohol (or *p*-nitrophenol) product becomes free, the $O_{Zn2}H^-$ performs the second nucleophilic attack on the phosphorus center to replace the Ser102 alkoxide.

To estimate the energetics of the protonation of methoxide (and *p*-nitrophenolate) bound by the AP active site, one water molecule was added to the phosphoseryl intermediates (**PSI_{me}** and **PSI_{pnp}**) to optimize the phosphoenzyme-alkoxide-water complexes (labeled by **PSI_{me}-W** and **PSI_{pnp}-W**, respectively) and the resulting phosphoenzyme-alcohol-hydroxide complexes (**PSI_{OH}-ME** and **PSI_{OH}-PNP**). They correspond to the species before and after protonation, respectively. In addition, the phosphoenzyme-hydroxide complex without alcohol (or *p*-nitrophenol) bound is referred to as **PSI_{OH}**. The protonation in the case of methyl phosphate is calculated to be an exother-

mic process (-8.0 kcal mol^{-1} with the solvation included, Figure 4). Considering the small endothermicity of the second chemical displacement step discussed below (2.4 kcal mol^{-1}), this leads to an overall reaction energy of 2.7 kcal mol^{-1} for the AP-catalyzed hydrolysis of methyl phosphate (see Figure 4). For another protonation possibility (i.e. the methoxide is directly expelled into the solution and gets protonated there), the proton transfer process seems to be feasible because water has a lower pK_a than methanol. However, the departure of negatively charged methoxide from the Zn2 cation appears to be difficult. In the optimization of phosphoenzyme-nitrophenol-hydroxide complex (**PSI$_{OH}$-PNP**), the proton of nitrophenol is, however, always transferred back to the $O_{Zn2}H^-$, leading to the phosphoenzyme-nitrophenolate-water complex (**PSI$_{pnp}$-W**). This probably indicates that no activation (protonation) of the leaving group is needed for the AP-catalyzed hydrolysis of *p*-nitrophenyl phosphate. It is thus postulated that the $O_{Zn2}H^-$ species is introduced from the solution. However, the release of *p*-nitrophenolate product from the Zn2 site is supposed to be endothermic, which will be discussed in the next section below.

After the alcohol product (or *p*-nitrophenolate) is released, the hydrolysis of phosphoseryl intermediate (**PSI**) takes place, that is, the Zn2-bound hydroxide ($O_{Zn2}H^-$) performs the nucleophilic attack on the phosphorus center to replace the Ser102 alkoxide. For all phosphate monoester substrates, this displacement step is identical as the nucleophile ($O_{Zn2}H^-$) and the leaving group (Ser102 alkoxide) are kept the same. The structure of the phosphoenzyme-hydroxide complex (**PSI$_{OH}$**) was optimized and is given in Figure 5. It can be found that, at **PSI$_{OH}$**, the Zn2 ion plays a role in stabilizing and orienting the hydroxide in the optimal position to attack the phosphorus center. In the **PSI$_{OH}$** structure, the distances of the nucleophile oxygen (O_{nuc}, the oxygen of $O_{Zn2}H^-$) to the P atom and the Zn2 ion are 3.32 and 1.92 Å, respectively. From **PSI$_{OH}$**, the transition state for the hydrolysis of **PSI** (referred to as **TS$_{hyd}$**, Figure 5) was located. At **TS$_{hyd}$**, the key distances of the P to the O_{nuc} and the leaving group oxygen (O_{lg}, the oxygen of Ser102 alkoxide) are 2.21 and 1.86 Å, respectively. A further investigation on the geometry of **TS$_{hyd}$** reveals that the two zinc ions may again stabilize the transition state, as the Zn1–O_{lg}, Zn1–O_{μ}, and Zn2–O_{μ} distances become shorter compared to the **PSI$_{OH}$** structure (Figure 5). The nature of **TS$_{hyd}$** was calculated by frequency analysis to be concerted with an imaginary frequency of 130*i* cm^{-1}. It turns out that, when the P–O_{nuc} bond is formed, the P–O_{lg} bond is dissociated and the proton of H_2O_{Mg} is delivered back to Ser102, leading to an Pi and the regenerated Ser102 residue and Mg-bound hydroxide ($O_{Mg}H^-$). The resulting enzyme-product complex (**Prod**) is given in Figure 5. Again, the overlaid structure (Figure S3) shows the high-degree structural consistency for the **PSI$_{OH}$**, **TS$_{hyd}$**, and **Prod** stationary points. The barrier and reaction energy of this step are calculated to be 16.0 and 2.3 kcal mol^{-1} including the solvation (Figure 4). The barrier is very close to the value estimated by kinetic experiments (16.2 kcal mol^{-1}, calculated from a rate constant of 0.6 s^{-1} at zero °C).[71]

The positions of stationary points in the corresponding MFJ plot (Figure 5) show that the hydrolysis of **PSI** also proceeds through a concerted associative path. It is also worth stressing that we did not observe any dissociative or stepwise associative pathways in this process.

2.5. Comparison with LFERs Experimental Results

As pointed out in ref. [51], traditional LFERs are empirical relationships and rather hard to reveal the nature of the reactions in a complicated system, because the shift of parabolas in different cases can lead to a similar LFER. Furthermore, LFERs are not able to distinguish between concerted and stepwise mechanisms. In contrast, if the landscape of the reacting system has been clearly described by locating the key transition states and by presenting the reaction pathways, it should be easy to determine the nature of the observed LFERs by shifting the parabolas. Based on the AP reaction mechanism and the PESs cal-

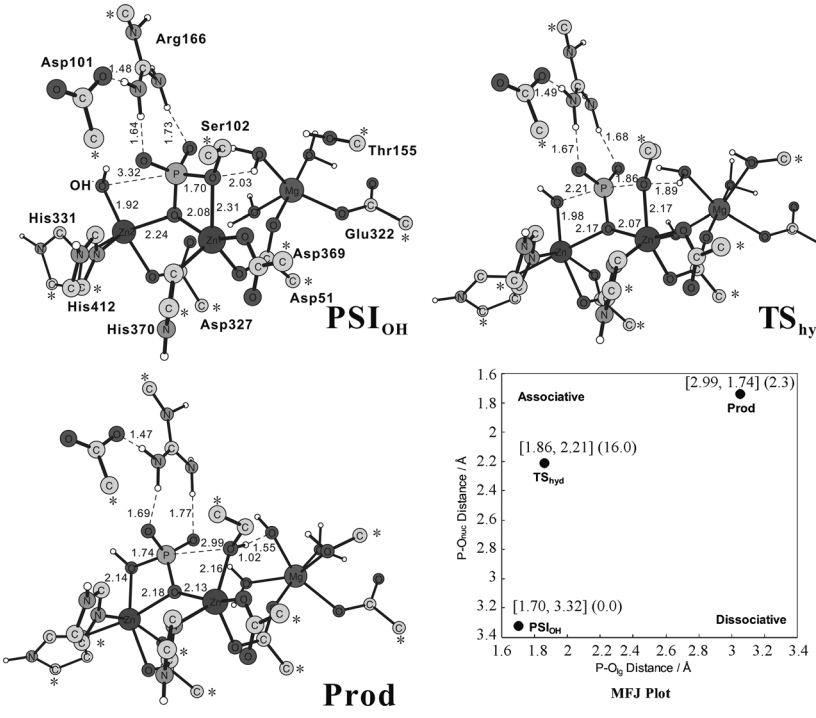

Figure 5. Optimized structures of stationary points in the hydrolysis of phosphoseryl intermediate and the corresponding More–O'Ferral–Jencks (MFJ) plot. For clarity, a few hydrogen atoms are omitted.

culated here (Figure 4), we tried to rationalize the LFERs observed in the experiments. The AP-catalyzed hydrolysis of both methyl and *p*-nitrophenyl phosphates can be considered as a reaction with two chemical steps, that is, phosphoryl transfer to enzyme and hydrolysis of **PSI**. Therefore, the hydrolysis of methyl phosphate is a two-step reaction with barriers of $\Delta E_1^{\neq} = 16.0$ kcal mol^{-1} and $\Delta E_2^{\neq} = 16.0$ kcal mol^{-1}, whereas the reaction of *p*-nitrophenyl phosphate has barriers of $\Delta E_1^{\neq} = 8.1$ kcal mol^{-1} and $\Delta E_2^{\neq} = 16.0$ kcal mol^{-1} (see Figure 4).

For alkyl phosphates, LFERs have been observed with a β_{lg} of -0.85 ± 0.1 (log k_{cat}/K_m vs. pK_a) by using the sensitive ^{32}P-labeled alkyl substrates.[6] The negative β_{lg} shows that the hydrolysis proceeds faster with the decrease of the pK_a of the leaving group. In this experiment, the substrate concentration is much smaller than that of the enzyme in order to ensure that each enzyme molecule is involved in at most one catalytic cycle and that the complication of product inhibition can be avoided. The k_{cat}/K_m was obtained by detecting the concentration of the phosphate product, indicating that both chemical steps should be taken into account when exploring the origin of k_{cat}/K_m. In the case of methyl phosphate, as considered in the present study (pK_a of methanol = 15.5), because the barriers for the two chemical steps are equivalent ($\Delta E_1^{\neq} = \Delta E_2^{\neq} = 16.0$ kcal mol^{-1}, Figure 4), both chemical steps (phosphoryl transfer and hydrolysis of **PSI**) contribute to the total reaction rate. Consequently, a small decrease in the pK_a value of the substrate leaving group should slightly lower the barrier of the phosphoryl transfer ($\Delta E_1^{\neq}$), thereby leading to a faster reaction rate. In addition, the barrier of the second step calculated here (16.0 kcal mol^{-1}, Figure 4) is quite close to a kinetic experimental estimation (16.2 kcal mol^{-1}, derived from a rate constant of 0.6 s^{-1} at zero °C).[71] Our calculations are thus in good agreement with the experimental observation. It should be pointed out that a quantitative clarification of LFERs requires the calculations of many different substrates, which is beyond the scope of the present study.

For aryl phosphates, in an improved kinetic experiment,[6] the k_{cat}/K_m was determined by monitoring the spectroscopy of the phenolate products, which are released after the first chemical step. It can therefore be concluded that the second step (hydrolysis of **PSI**) does not contribute to the reported k_{cat}/K_m. In the case of *p*-nitrophenyl phosphate (pK_a of *p*-nitrophenol = 7.1), the barrier for phosphoryl transfer to enzyme is calculated to be 8.1 kcal mol^{-1}, which is 7.9 kcal mol^{-1} lower than that for methyl phosphate (Figure 4). This is consistent with the sign of β_{lg}, that is, a leaving group with a lower pK_a should have a lower barrier. The low barrier for this first step implies that the phenolate release from the zinc site may also contribute to the rate limiting step. The driving force for the hydrolysis of *p*-nitrophenyl phosphate was measured to be about 4 kcal mol^{-1};[72] together with the large exothermicity for the first step (15.2 kcal mol^{-1}) this suggests that some energetic penalty is present for the release of *p*-nitrophenolate. Thus, the reaction rate of the hydrolysis of aryl phosphates should only be determined by the release of phenolate products from the AP-active site and k_{cat}/K_m is almost the same for diverse phenyl phosphates, as observed in experiments.[6]

3. Conclusions

In this paper, we have reported a theoretical examination of the catalytic mechanism of alkaline phosphatase (AP) by using DFT. The AP-catalyzed hydrolysis of methyl and *p*-nitrophenyl phosphates (as the models of alkyl and aryl phosphates, respectively) was investigated with an active-site model constructed on the basis of an X-ray crystal structure of AP. The transition states and intermediates along the reaction pathways were optimized and characterized. The potential energy surfaces for the AP-catalyzed reactions of methyl and *p*-nitrophenyl phosphates were plotted (Figure 4).

The calculations presented here confirm that the AP reaction employs a "ping-pong" mechanism involving two chemical displacement steps (shown in Scheme 2). The Ser102 alkoxide activated by an Mg-bound hydroxide first performs the nucleophilic attack on the phosphorus center to replace the leaving group (i.e. phosphoryl transfer), and the Ser102 alkoxide is subsequently displaced by a Zn2-bound hydroxide (i.e. hydrolysis of phosphoseryl intermediate). In this mechanism, a covalent phosphoseryl intermediate (**PSI**) is formed and the configuration at phosphorus center is retained in the catalytic cycle.

Both displacement steps proceed through a concerted associative pathway no matter which substrate is employed (methyl or *p*-nitrophenyl phosphate), although the nature of the phosphoryl transfer trends towards the dissociative direction with the decrease of the pK_a of the substrate leaving group. No dissociative mechanism for methyl or *p*-nitrophenyl phosphate hydrolysis was found in this work, although many attempts have been made. A possible reason is that the parts directly binding to the phosphate moiety are all positively charged, including Arg166, Zn1, and Zn2. This local cationic surrounding most likely prefers an associative mechanism, in which negative charge is increased during the catalysis.[23] The same findings have been obtained in the case of phosphotriesterase (PTE), another di-zinc enzyme that catalyzes the hydrolysis of phosphotriesters via a stepwise associative pathway.[39–41] In addition, the observation of an associative mechanism could be partially due to the methodology used, in which certain key atoms were fixed during geometry optimizations and the flexibility of the model could be somewhat underestimated. However, the effect of coordinate locking is expected to be quite small and it has been shown in the case of PTE that the conclusion of a stepwise associative mechanism is not changed no matter whether the locking of atoms was applied or not.[41] Our proposal of a concerted associative mechanism for AP is consistent with a recent QM/MM investigation on the *p*-nitrophenyl phosphate hydrolysis, in which a concerted but slightly loose transition state was observed for R166S AP.[19] On the other hand, a different QM/MM study of the *p*-nitrophenyl phosphate hydrolysis has shown that different sizes of the QM subsystem can render to different mechanisms, either associative or dissociative ones.[34]

The roles of the two zinc ions can be evaluated by studying how some important geometric parameters change during the reactions. The two zinc ions are revealed to be able to stabilize the transition state structures. Zn2 also plays a role in stabiliz-

ing the negative charge that develops at the substrate leaving group, consequently facilitating the first step of phosphoryl transfer. During catalysis, the distance between two zinc ions (Zn1–Zn2) does not show obvious fluctuation with short Zn1–Zn2 distances in the transition states (~4.0 Å, see Table S1), a result very close to a recent QM/MM study by Hou and Cui.[17] It should be noted that this is different from the calculations using the semiempirical method of AM1/d-PhoT, with which the Zn1–Zn2 distance was found to vary significantly during the reaction for both mono- and diester substrates, and which has been attributed to the promiscuity of the enzyme by the authors.[18,34,73]

The present calculations agree well with the LFERs experimental results. In particular, it has been demonstrated here that, in the AP-catalyzed hydrolysis of alkyl phosphates, both chemical displacement steps (phosphoryl transfer and hydrolysis of **PSI**) contribute to the rate-limiting step as the barriers of the two steps are very close ($\Delta E_1^{\neq} = \Delta E_2^{\neq} = 16.0$ kcal mol^{-1} for methyl phosphate, Figure 4). A small change in the leaving group (i.e. pK_a) results in the variation of k_{cat}/K_m. For aryl phosphates, the first chemical step has a much lower barrier than that of the second step ($\Delta E_1^{\neq} = 8.1$ kcal mol^{-1} and $\Delta E_2^{\neq} =$ 16.0 kcal mol^{-1} for *p*-nitrophenyl phosphate, Figure 4) and the phenolate release from the Zn2 site is considered to be rate-limiting. This is consistent with the experimental observation that the adjustment of the pK_a of the substrate leaving group hardly affects k_{cat}/K_m for the aryl phosphate hydrolysis.[6,31]

Finally, the results of this paper offer an effective verification of the usefulness and powerfulness of quantum chemical active-site modeling methodology in the exploration of enzyme reaction mechanisms and in the characterization of transition states involved. In particular, the small energetic difference for the cluster model with and without continuum solvation (see Figure 4) implies that most of the polarization responsible for the reaction has already been captured by the present active-site model and evaluated by high-level quantum mechanics.

Acknowledgements

We thank Prof. Fahmi Himo (Stockholm University) for valuable discussions and help and Dr. Sven de Marothy (Stockholm University) for providing the graphic program used to make Figures 2, *3, and 5 in this paper. This work was financially supported by the Major State Basic Research Development Programs of China (2011CBA00701), the National Natural Science Foundation of China (21103010, 21373027), the 111 Project (B07012), the Excellent Young Scholars Research Fund of Beijing Institute of Technology (2010Y1214), the Basic Research Fund of Beijing Institute of Technology (20101742032), and Beijing Key Laboratory for Chemical Power Source and Green Catalysis (2013CX02031).*

Keywords: alkaline phosphatase · associative mechanism · density functional calculations · enzyme catalysis · phosphate ester hydrolysis

[1] J. E. Coleman, *Annu. Rev. Biophys. Biomol. Struct.* **1992**, *21*, 441 – 483.
[2] J. H. Schwartz, F. Lipmann, *Proc. Natl. Acad. Sci. USA* **1961**, *47*, 1996 – 2005.
[3] S. R. Jones, L. A. Kindman, J. R. Knowles, *Nature* **1978**, *275*, 564 – 565.
[4] N. S. Terefe, J. M. Arimi, A. V. Loey, M. Hendrickx, *Biotechnol. Prog.* **2004**, *20*, 1467 – 1478.
[5] T. T. Simopoulos, W. P. Jencks, *Biochemistry* **1994**, *33*, 10375 – 10380.
[6] P. J. O'Brien, D. Herschlag, *Biochemistry* **2002**, *41*, 3207 – 3225.
[7] P. J. O'Brien, D. Herschlag, *Biochemistry* **2001**, *40*, 5691 – 5699.
[8] J. G. Zalatan, D. Herschlag, *J. Am. Chem. Soc.* **2006**, *128*, 1293 – 1303.
[9] N. Sträter, W. N. Lipscomb, T. Klabunde, B. Krebs, *Angew. Chem. Int. Ed.* **1996**, *35*, 2024 – 2055.
[10] W. N. Lipscomb, N. Sträter, *Chem. Rev.* **1996**, *96*, 2375 – 2433.
[11] D. E. Wilcox, *Chem. Rev.* **1996**, *96*, 2435 – 2458.
[12] G. Parkin, *Chem. Rev.* **2004**, *104*, 699 – 767.
[13] J. Weston, *Chem. Rev.* **2005**, *105*, 2151 – 2174.
[14] K. M. Holtz, E. R. Kantrowitz, *FEBS Lett.* **1999**, *462*, 7 – 11.
[15] D. E. Fenton, H. Okawa, *J. Chem. Soc. Dalton Trans.* **1993**, 1349 – 1357.
[16] T. W. Reid, I. B. Wilson, *The Enzymes* (Eds: P. D. Boyer), Academic Press, New York, **1971**, pp. 373 – 415.
[17] G. Hou, Q. Cui, *J. Am. Chem. Soc.* **2012**, *134*, 229 – 246.
[18] V. López-Canut, M. Roca, J. Bertrán, V. Moliner, I. Tuñón, *J. Am. Chem. Soc.* **2011**, *133*, 12050 – 12062.
[19] G. Hou, Q. Cui, *J. Am. Chem. Soc.* **2013**, *135*, 10457 – 10469.
[20] B. Stec, K. M. Holtz, E. R. Kantrowitz, *J. Mol. Biol.* **2000**, *299*, 1303 – 1311.
[21] K. M. Holtz, B. Stec, E. R. Kantrowitz, *J. Biol. Chem.* **1999**, *274*, 8351 – 8354.
[22] J. E. Murphy, B. Stec, L. Ma, E. R. Kantrowitz, *Nat. Struct. Biol.* **1997**, *4*, 618 – 622.
[23] K. M. Holtz, I. E. Catrina, A. C. Hengge, E. R. Kantrowitz, *Biochemistry* **2000**, *39*, 9451 – 9458.
[24] P. J. O'Brien, D. Herschlag, *J. Am. Chem. Soc.* **1999**, *121*, 11022 – 11023.
[25] E. R. Kantrowitz, *Handbook of Metalloproteins, Vol. 3* (Eds: A. Messerschmidt, M. Cygler, W. Bode), John Wiley&Sons Ltd., Chichester, **2004**, 76.
[26] I. Bertini, C. Luchinat, *Bioinorganic Chemistry* (Eds: I. Bertini, H. B. Gray, S. J. Lippard, J. S. Valentine), University Science Books, Sausalito, **1994**, 88.
[27] M. Fothergill, M. F. Goodman, J. Petruska, A. Warshel, *J. Am. Chem. Soc.* **1995**, *117*, 11619 – 11627.
[28] G. L. Borosky, S. Lin, *J. Chem. Inf. Model.* **2011**, *51*, 2538 – 2548.
[29] F. Hollfelder, D. Herschlag, *Biochemistry* **1995**, *34*, 12255 – 12264.
[30] A. D. Hall, A. Williams, *Biochemistry* **1986**, *25*, 4784 – 4790.
[31] R. Han, J. E. Coleman, *Biochemistry* **1995**, *34*, 4238 – 4245.
[32] A. D. Hall, A. Williams, *J. Chem. Soc. Chem. Commun.* **1985**, 1680 – 1681.
[33] J. Florián, A. Warshel, *J. Phys. Chem. B* **1998**, *102*, 719 – 734.
[34] V. López-Canut, S. Martí, J. Bertrán, V. Moliner, I. Tuñón, *J. Phys. Chem. B* **2009**, *113*, 7816 – 7824.
[35] A. D. Becke, *J. Chem. Phys.* **1993**, *98*, 1372 – 1377.
[36] A. D. Becke, *J. Chem. Phys.* **1993**, *98*, 5648 – 5652.
[37] C. Lee, W. Yang, R. G. Parr, *Phys. Rev. B* **1988**, *37*, 785 – 789.
[38] F. Duarte, B. A. Amrein, S. C. L. Kamerlin, *Phys. Chem. Chem. Phys.* **2013**, *15*, 11160 – 11177.
[39] S. L. Chen, W. H. Fang, F. Himo, *J. Phys. Chem. B* **2007**, *111*, 1253 – 1255.
[40] J. Kim, P. C. Tsai, S. L. Chen, F. Himo, S. C. Almo, F. M. Raushel, *Biochemistry* **2008**, *47*, 9497 – 9504.
[41] S. L. Chen, W. H. Fang, F. Himo, *Theor. Chem. Acc.* **2008**, *120*, 515 – 522.
[42] S. L. Chen, T. Marino, W. H. Fang, N. Russo, F. Himo, *J. Phys. Chem. B* **2008**, *112*, 2494 – 2500.
[43] S. L. Chen, W. H. Fang, F. Himo, *J. Inorg. Biochem.* **2009**, *103*, 274 – 281.
[44] M. Leopoldini, N. Russo, M. Toscano, *J. Am. Chem. Soc.* **2007**, *129*, 7776 – 7784.
[45] M. E. Alberto, M. Leopoldini, N. Russo, *Inorg. Chem.* **2011**, *50*, 3394 – 3403.
[46] A. J. M. Ribeiro, M. E. Alberto, M. J. Ramos, P. A. Fernandes, N. Russo, *Chem. Eur. J.* **2013**, *19*, 14081 – 14089.
[47] T. Marino, N. Russo, M. Toscano, *Chem. Eur. J.* **2013**, *19*, 2185 – 2192.
[48] T. Marino, N. Russo, M. Toscano, *Inorg. Chem.* **2013**, *52*, 655 – 659.
[49] A. J. M. Ribeiro, M. J. Ramos, P. A. Fernandes, N. Russo, *Chem. Phys. Lett.* **2013**, *571*, 66 – 70.
[50] R.-Z. Liao, J.-G. Yu, F. Himo, *Inorg. Chem.* **2010**, *49*, 6883 – 6888.

[51] M. Klähn, E. Rosta, A. Warshel, *J. Am. Chem. Soc.* **2006**, *128*, 15310 – 15323.
[52] E. Rosta, S. C. L. Kamerlin, A. Warshel, *Biochemistry* **2008**, *47*, 3725 – 3735.
[53] Gaussian 03 (Revision D.01), M. J. Frisch, G. W. Trucks, H. B. Schlegel, G. E. Scuseria, M. A. Robb, J. R. Cheeseman, J. A. Montgomery, Jr., T. Vreven, K. N. Kudin, J. C. Burant, J. M. Millam, S. S. Iyengar, J. Tomasi, V. Barone, B. Mennucci, M. Cossi, G. Scalmani, N. Rega, G. A. Petersson, H. Nakatsuji, M. Hada, M. Ehara, K. Toyota, R. Fukuda, J. Hasegawa, M. Ishida, T. Nakajima, Y. Honda, O. Kitao, H. Nakai, M. Klene, X. Li, J. E. Knox, H. P. Hratchian, J. B. Cross, V. Bakken, C. Adamo, J. Jaramillo, R. Gomperts, R. E. Stratmann, O. Yazyev, A. J. Austin, R. Cammi, C. Pomelli, J. W. Ochterski, P. Y. Ayala, K. Morokuma, G. A. Voth, P. Salvador, J. J. Dannenberg, V. G. Zakrzewski, S. Dapprich, A. D. Daniels, M. C. Strain, O. Farkas, D. K. Malick, A. D. Rabuck, K. Raghavachari, J. B. Foresman, J. V. Ortiz, Q. Cui, A. G. Baboul, S. Clifford, J. Cioslowski, B. B. Stefanov, G. Liu, A. Liashenko, P. Piskorz, I. Komaromi, R. L. Martin, D. J. Fox, T. Keith, M. A. Al-Laham, C. Y. Peng, A. Nanayakkara, M. Challacombe, P. M. W. Gill, B. Johnson, W. Chen, M. W. Wong, C. Gonzalez, J. A. Pople, Gaussian, Inc., Wallingford, CT, **2004**.
[54] A. Klamt, G. Schüürmann, *J. Chem. Soc. Perkin. Trans.* 2, **1993**, 799 – 805.
[55] R. Cammi, B. Mennucci, J. Tomasi, *J. Phys. Chem. A* **1999**, *103*, 9100 – 9108.
[56] V. Barone, M. Cossi, *J. Phys. Chem. A* **1998**, *102*, 1995 – 2001.
[57] J. Tomasi, B. Mennucci, R. Cammi, *Chem. Rev.* **2005**, *105*, 2999 – 3093.
[58] P. E. M. Siegbahn, M. R. A. Blomberg, *Chem. Rev.* **2000**, *100*, 421 – 437.
[59] R. Sevastik, F. Himo, *Bioorg. Chem.* **2007**, *35*, 444 – 457.
[60] K. H. Hopmann, F. Himo, *J. Chem. Theory Comput.* **2008**, *4*, 1129 – 1137.
[61] P. Georgieva, F. Himo, *J. Comput. Chem.* **2010**, *31*, 1707 – 1714.
[62] R. Z. Liao, J. G. Yu, F. Himo, *J. Chem. Theory Comput.* **2011**, *7*, 1494 – 1501.
[63] R. Z. Liao, W. Thiel, *J. Phys. Chem. B* **2013**, *117*, 3954 – 3961.
[64] E. Bobyr, J. K. Lassila, H. I. Wiersma-Koch, T. D. Fenn, J. J. Lee, I. Nikolic-Hughes, K. O. Hodgson, D. C. Rees, B. Hedman, D. Herschlag, *J. Mol. Biol.* **2012**, *415*, 102 – 117.
[65] I. B. Wilson, J. Dayan, *Biochemistry* **1965**, *4*, 645 – 649.
[66] P. Gettins, J. E. Coleman, *J. Biol. Chem.* **1983**, *258*, 408 – 416.
[67] W. P. Jencks, *Chem. Rev.* **1985**, *85*, 511 – 527.
[68] R. A. More, O'Ferrall, *J. Chem. Soc. B* **1970**, 274 – 277.
[69] I. Nikolic-Hughes, D. C. Rees, D. Herschlag, *J. Am. Chem. Soc.* **2004**, *126*, 11814 – 11819.
[70] W. P. Jencks, J. Regenstein, *Handbook of Biochemistry and Molecular Biology*, CRC, Cleveland, OH, **1976**.
[71] P. J. O'Brian, J. K. Lassila, T. D. Fenn, J. G. Zalatan, D. Herschlag, *Biochemistry* **2008**, *47*, 7663 – 7672.
[72] R. N. Goldberg, B. E. Lang, C. Lo, D. J. Ross, Y. B. Tewari, *J. Chem. Thermodyn.* **2009**, *41*, 654 – 665.
[73] V. López-Canut, M. Roca, J. Bertrán, V. Moliner, I. Tuñón, *J. Am. Chem. Soc.* **2010**, *132*, 6955 – 6963.

Received: February 7, 2014
Revised: February 25, 2014
Published online on March 28, 2014